FULL PAPER

Splitting dioxygen over distant binuclear transition metal cationic sites in zeolites. Effect of the transition metal cation

Jiri Dedecek[1] | Edyta Tabor[1] | Prokopis C. Andrikopoulos[1,2] | Stepan Sklenak[1] 🔘

[1]J. Heyrovský Institute of Physical Chemistry, The Czech Academy of Sciences, Prague, Czech Republic
[2]Institute of Biotechnology, The Czech Academy of Sciences, The Czech Academy of Sciences, BIOCEV, Prumyslova 595, 25250 Vestec, Prague, Czech Republic

Correspondence
Stepan Sklenak, J. Heyrovský Institute of Physical Chemistry, The Czech Academy of Sciences, Dolejskova 3, 18223 Prague, Czech Republic.
Email: stepan.sklenak@jh-inst.cas.cz

Funding information
Akademie Věd České Republiky, Grant/Award Number: 61388955; Grantová Agentura České Republiky, Grant/Award Numbers: 17-00742S, 19-02901S

Abstract

Splitting dioxygen to yield highly active oxygen species attracts enormous attention due to its potential in direct oxidation reactions, mainly in transformation of methane into valuable products. Distant binuclear cationic Fe(II) centers in Fe-ferrierite have recently been shown to be active in splitting dioxygen at room temperature to form very active oxygen species able to oxidize methane to methanol at room temperature as well. Computational models of the distant binuclear transition metal cationic sites (Co(II), Mn(II), and Fe(II)) stabilized in the ferrierite matrix were investigated by periodic density-functional theory calculations including molecular dynamics simulations. The results reveal that the M(II) cations capable of the M(II) → M(IV) redox cycle with the M...M distance of ca 7.4 Å stabilized in two adjacent β sites of ferrierite can split dioxygen. Our study opens the possibility of developing tunable zeolite-based systems for the activation of dioxygen employed for direct oxidations.

KEYWORDS
alpha oxygen, density functional calculations, splitting dioxygen, VASP, zeolites

1 | INTRODUCTION

The activation of dioxygen for its application as an eco-friendly, and low-cost oxidant represents one of the greatest challenges in chemical technology [1–4]. Methane represents the dominant component of natural and shale gases and its transformation into liquid valuable products as methanol is in high demand. Naturally occurring systems are able to activate dioxygen for direct oxidation of methane to methanol over methane monooxygenase [5]. However, there is no technology available that oxidizes methane directly to methanol with dioxygen in satisfactory yields. Methane is transformed into synthesis gas (H_2 and CO) which is subsequently either catalytically converted to methanol or by Fischer–Tropsch synthesis processed into liquid hydrocarbons [6]. Thus, processing methane to valuable products is energetically, technologically, and investably very demanding. Concluding, the direct route of oxidation of methane to methanol would represent a significant step ahead in methane utilization if employing a cheap oxidant such as dioxygen. Recently, intensive research in this area has been focused on the activity of Fe and Cu cations stabilized in aluminosilicate matrices of zeolites. Currently, the most efficient catalysts are Cu cations and Cu oxide clusters stabilized in zeolite matrices. However, they still show a very low methanol productivity over these systems both in cyclic stoichiometric and continuous modes [2–3, 7–10]. In addition, steam has to be employed to release methanol into the gas phase. Subsequently, the presence of water vapor leads to a blockage and destruction of the active centers. Thus, the zeolite catalysts under these conditions are not suitable for methane transformations at the industrial scale. The previously discovered activity [11] regarding the direct oxidation of methane to methanol over isolated Fe cations stabilized in zeolite matrices by the α-oxygen formed by the decomposition of N_2O is highly inspirational. However, it is only of academic interest and does not represent a real basis for a possible technological application either.

Very recently, a breakthrough [12] in the activation of dioxygen [4] has been achieved. The distant binuclear cationic Fe(II) centers in Fe-ferrierite are on the one hand close enough to cooperate in a four electron process of the activation of dioxygen but on the other hand far enough that a formation of an oxo-bridge species known for metalloenzymes [4,5] is not possible and splitting dioxygen occurs even at room temperature [4]. The cleavage of dioxygen results in the formation of a pair of very active oxygen species called the α-oxygen (i.e., [Fe(IV) = O]$^{2+}$) [1, 4, 13–15].

The α-oxygen formed on isolated Fe cations is known for its exceptional properties regarding the direct oxidation of methane to methanol [11, 16] and benzene to phenol [17, 18]. However, until now it has been possible to prepare the α-oxygen exclusively by the abstraction of the oxygen atom from N_2O over isolated iron species in ZSM-5 [11, 16–19], ferrierite [13–15], SSZ-13 [20], and the beta zeolite [1, 19]. Furthermore, we have also shown the corresponding exceptional oxidation properties of the α-oxygen atoms created on distant binuclear Co(II) and Ni(II) centers accommodated in the adjacent β cationic sites [21–23] of ferrierite formed by the decomposition of N_2O [15]. Moreover, the unique oxidation properties concerning the direct oxidation of methane to methanol at room temperature were recently confirmed also for a pair of the α-oxygen atoms prepared by splitting dioxygen over the distant binuclear Fe(II) sites stabilized in the adjacent β cationic sites of the ferrierite matrix [4]. These oxidized centers when employed for the direct oxidation of methane to methanol feature an additional advantage that is an easy release of the oxidation products from the system without the necessity of water or water-organic medium extraction of the oxidation products [4, 15]. These results make the distant binuclear Fe(II) sites stabilized in a zeolite matrix a highly promising material for the direct methane oxidation [4, 15].

The density-functional theory (DFT) calculated barriers of splitting dioxygen (25 kcal/mol) [4] and abstracting oxygen from N_2O (15 kcal/mol) [15] over Fe-ferrierite reveal facile oxidations of the Fe(II) cations of Fe-ferrierite to yield the α-oxygen. However, Fe(II) cations are sensitive to the conditions of (a) the introduction into the zeolite matrix and (b) the reaction. Therefore, it is very difficult to prepare highly loaded Fe(II) zeolites with the exclusive presence of bare Fe(II) cations. Thus, there is an important question whether splitting dioxygen is unique to distant binuclear Fe(II) sites or represents a general property of transition metal cations able to perform the M(II) → M(IV) redox cycle when arranged in the distant binuclear site. If the latter is true, it opens the possibility of the development of exceptionally active and tunable systems with higher concentrations of the active sites for the direct oxidation of methane.

In this article, we use periodic DFT calculations to investigate the effect of the type of transition metal cation (Co(II), Mn(II), and Fe(II)) accommodated in the adjacent β cationic sites of ferrierite on the activity of the distant binuclear M(II) sites in splitting dioxygen and the mechanism of the cleavage of dioxygen. The obtained results clearly evidence that the capability of splitting dioxygen is most likely a general feature of the distant binuclear M(II) sites of cations able to carry out the M(II) → M(IV) redox cycle. This result suggests the possibility of developing highly active tunable systems capable of splitting dioxygen. Such substances represent a base for the development of materials for the direct oxidation of methane or even bulkier molecules.

2 | COMPUTATIONAL MODELS AND METHODS

2.1 | Computational models

Two models, Co-FER and Mn-FER, featuring a super cell composed of two unit cells along the c dimension (i.e., $a = 18.651$, $b = 14.173$, and $c = 14.808$ Å) with the P1 symmetry are used for the distant binuclear Me(II) (Me(II) = Co(II) and Mn(II), respectively) centers. Each model contains four Al/Si substitutions forming two $\beta2$ sites [4, 14, 15, 21, 24] with the four Al atoms located in the T2 [25] sites of the two adjacent six rings accommodating two Me(II) cations. The starting structure was generated from the experimental structure (orthorhombic, space group Immm, cell parameters $a = 18.651$, $b = 14.173$, and $c = 7.404$ Å) of ferrierite determined by neutron diffraction [26].

2.2 | Electronic structure calculations

Periodic DFT calculations were carried out by using the Vienna Ab initio Simulation Package (VASP) code [27–30]. The high-spin electron configuration d5↑d2↓ was used for the Co species of the Co-FER model. The high-spin electron configuration d5↑d0↓ and other possible spin states were employed for the Mn species of the Mn-FER model. The spin state S ($S = N/2$; N is the number of unpaired electrons) was fixed during the molecular dynamics (MD) simulations and optimizations. Moreover, for all the optimized structures for both the Co-FER and Mn-FER models, the spin state used was verified that it really corresponds to the ground state. The Kohn–Sham equations were solved variationally in a plane-wave basis set using the projector-augmented wave method of Blöchl [31], as adapted by Kresse and Joubert [32]. The exchange-correlation energy was described by the Perdew–Burke–Ernzerhof [33] generalized gradient approximation functional. Brillouin zone sampling was restricted to the Γ point. A plane-wave cutoff of 600 eV and the density-dependent energy correction (dDsC) dispersion correction [34, 35] were used for the geometry optimizations, and a smaller cutoff of 400 eV and the DFT-D2 method [36] were used for the MD simulations.

2.3 | Molecular dynamics

MD simulations were carried out on the Co-FER and Mn-FER models. The MD computations used the exact Hellmann-Feynman forces acting on atoms and applied the statistics of canonical ensemble to the motion of the atomic nuclei [37] by using the Verlet velocity algorithm [38, 39] to

integrate Newton's equations of motion. The time step for the integration of the equations of motion was 1 fs. The simulations were run for 10 000 fs at 400 K. Visual inspection of the structures along the MD trajectories showed that the duration of the MD simulations was long enough, because it included both the rearrangements of the local structures of the ferrierite framework (up to ca. 2000 fs) and a long period (ca. 8000 fs) when the system fluctuated around the equilibrium and "snapshots" were collected and optimized. Similar time lengths were used for MD simulations of cationic sites in zeolites [4, 15, 40–42]. The MD simulations serve to obtain the rearranged local structures (details are provided in our prior studies [14, 24]). The rearrangement can be monitored by visual inspection. No physical quantity is derived from the MD trajectories. The structures of 20 distinct snapshots collected at 500, 1000, 1500, … 10 000 fs of the MD simulations were optimized for the two computational models.

2.4 | Geometry optimizations

The collected snapshots were optimized. The atomic positions were optimized at constant volume by using a conjugate-gradient algorithm minimization of energies and forces, whereas the lattice parameters were fixed at their experimental values. The 20 optimized snapshots differ in the structure and energy and only the most stable structure for each of the two investigated models was then used for the subsequent calculations.

3 | RESULTS

3.1 | Splitting dioxygen over the distant binuclear Co(II) sites

An $O_2(g)$ molecule that is in a triplet state adsorbs on one of the Co(II) cations to yield a [Co OO_{mono}…Co]′ monodentate complex **2′** with the O_2 moiety in a triplet state. The calculated adsorption energy is −6.5 kcal/mol. **2′** either undergoes a spin crossover to give a [Co OO_{mono}…Co] monodentate complex **2** (the energy drops by 3.3 kcal/mol) which has the O_2 moiety in a singlet state, or rearranges its structure to form a [Co OO_{bi}…Co]′ bidentate complex **3′** (the calculated adsorption energy is −4.9 kcal/mol). In the latter case, a spin change occurs and a [Co OO_{bi}…Co] bidentate complex **3** with the O_2 moiety in a singlet state is yielded. **3** is more stable than **3′** by 5.6 kcal/mol. The bidentate complex **3** is more stable, however, the O_2 moiety of the slightly less stable monodentate complex **2** is better positioned for the interaction with the other Co(II) located in the adjacent $\beta2$ site. Subsequently, dioxygen is cleaved via a [Co—O—O—Co] transition state **TS** to yield a [Co=O O=Co] complex **4** in a concerted manner. Both Co in **4** are oxidized to form a pair of the α-oxygen atoms. The calculated reaction energy of the reaction from **1** + $O_2(g)$ to give **4** is −13.4 kcal/mol (Table 1). The calculated barrier of the cleavage of dioxygen is 24.3 kcal/mol (Table 1), indicating that splitting dioxygen should be facile.

The optimized structures of **1**, **2**, **3**, **TS**, and **4** and the energy profile of splitting dioxygen are shown in Figure 1.

3.2 | Splitting dioxygen over the distant binuclear Mn(II) sites

An $O_2(g)$ molecule that is in a triplet state adsorbs on one of the Mn(II) cations of **1** (S = 10/2) and a spin change occurs concomitantly on the Mn(II) cation with the adsorbed O_2 to yield a [Mn OO_{mono}…Mn]′ monodentate complex **2′** (S = 10/2) with the O_2 moiety in a triplet state. The calculated adsorption energy is −11.3 kcal/mol. **2′** either undergoes a spin crossover to give a [Mn OO_{mono}…Mn] monodentate complex **2** (S = 8/2) which has the O_2 moiety in a singlet state releasing 6.2 kcal/mol, or rearranges its structure to form a [Mn OO_{bi}…Mn]′ bidentate complex **3′** (S = 10/2) releasing 1.9 kcal/mol. In the latter case, a spin change occurs and a [Mn OO_{bi}…Mn] bidentate complex **3** (S = 8/2) with the O_2 moiety in a singlet state is yielded. **3** is more stable than **3′** by 8.1 kcal/mol. The bidentate complex **3** is more stable, however, the O_2 moiety of the less

TABLE 1 Barrier ΔE_{ACT1},[a] reaction energy ΔE_R,[b] reverse barrier ΔE_{ACT2},[c] and $\Delta\Delta E_{ACT}$ (i.e., $\Delta E_{ACT2} - \Delta E_{ACT1}$)

Model	ΔE_{ACT1}	ΔE_R	ΔE_{ACT2}	$\Delta\Delta E_{ACT}$
Co-FER	24.3	−13.4	27.2	2.9
Mn-FER	36.8	−28.4	43.9	7.1
Fe-FER[d]	24.9	−24.7	28.0	3.1

Note: The energies are in kcal/mol.
[a]The calculated barrier of the cleavage of dioxygen.
[b]The reaction energy of splitting dioxygen (i.e., the reaction from **1** + $O_2(g)$ to give **4**).
[c]The calculated barrier of the recombination of dioxygen (i.e., **4** to yield **3**).
[d]The data for the Fe-FER model are taken from our prior study [4].
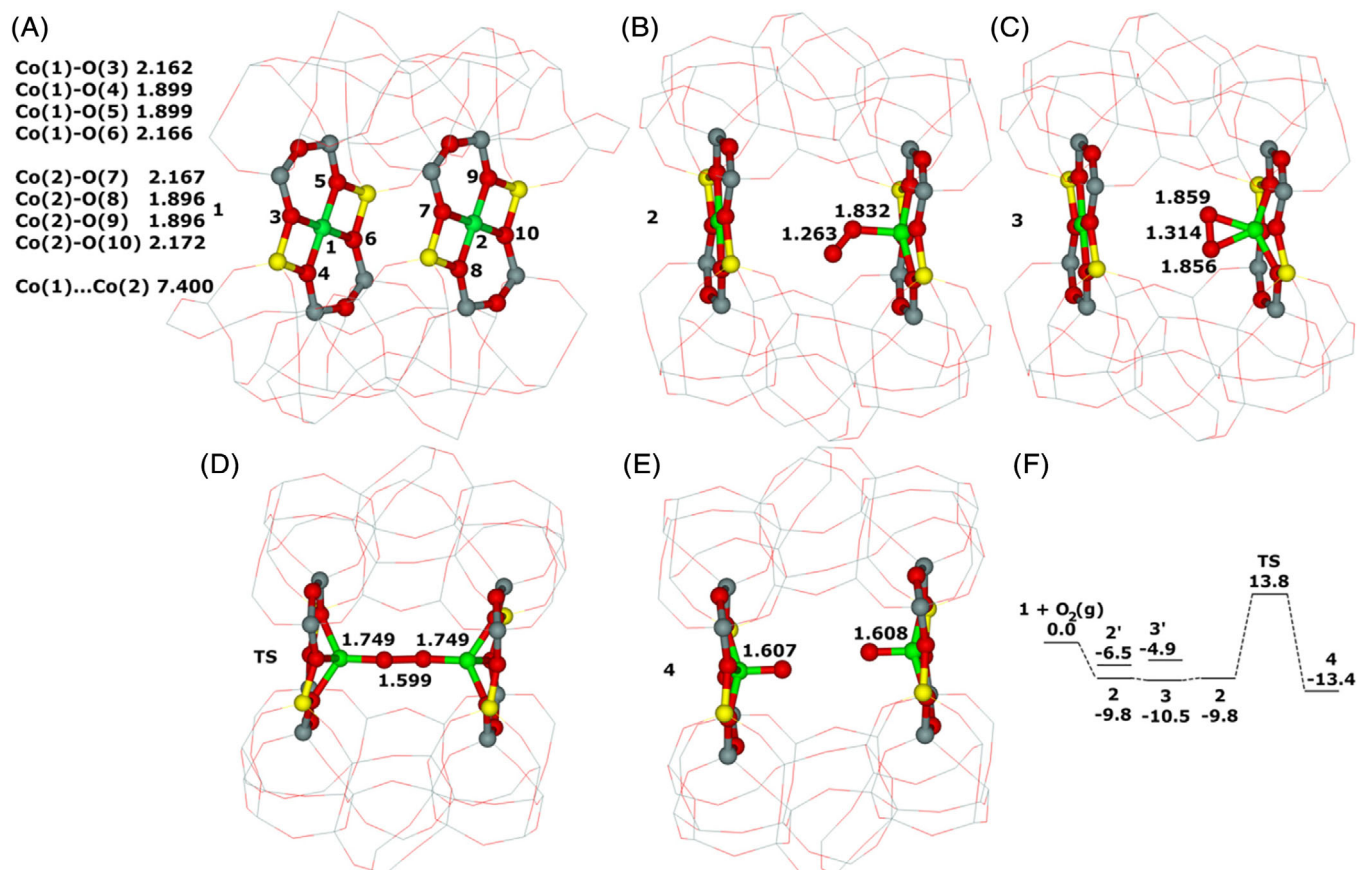
FIGURE 1 Co-FER model. Optimized structures for (A) the two adjacent $\beta2$ sites of Co-ferrierite **1** after molecular dynamics (MD) simulations, (B) the monodentate [Co OO$_{mono}$...Co] complex **2**, (C) the bidentate [Co OO$_{bi}$...Co] complex **3**, (D) the [Co—O—O—Co] transition state **TS**, and (E) the [Co=O O=Co] product **4**. The distances are in Å. Silicon atoms are in gray, oxygen atoms in red, aluminum atoms in yellow, and cobalt atoms in green. Schematic energy profile (in kilocalorie per mol) for the spin state $S = 6/2$ (2′ and 3′ are $S = 8/2$) for (F) the formation of the Co=O O=Co product **4**

stable monodentate complex **2** is better positioned for the interaction with the other Mn(II) located in the adjacent $\beta2$ site. Subsequently, dioxygen is cleaved via a [Mn—O—O—Mn] transition state **TS** ($S = 8/2$) to yield a [Mn=O O=Mn]′ complex **4**′ ($S = 8/2$) in a concerted manner. The formation of **4**′ is slightly endothermic by 0.8 kcal/mol but **4**′ undergoes a spin crossover to give **4** ($S = 6/2$) which is more stable than **4**′ by 29.2 kcal/mol. Both Mn in **4** are oxidized to form a pair of the α-oxygen atoms. The calculated reaction energy of the reaction from **1** + O_2(g) to give **4** is −28.4 kcal/mol (Table 1). The calculated barrier of the cleavage of dioxygen is 36.8 kcal/mol (Table 1), indicating that splitting dioxygen is sluggish. The optimized structures of **1**, **2**, **3**, **TS**, and **4** and the energy profile of splitting dioxygen are shown in Figure 2.

4 | DISCUSSION

The optimized structures of **1**, **2**, **3**, **TS**, and **4** and the energy profile of splitting dioxygen are shown in Figure 3 for the Fe-FER model of our prior study [4] for better clarity and intelligibility of Discussion.

Our periodic DFT calculations show that all the three M(II) (M(II) = Co(II), Fe(II), and Mn(II)) cations accommodated in two adjacent $\beta2$ sites of ferrierite are able to cleave dioxygen to yield a pair of the α-oxygen atoms. The calculated reaction mechanisms are the same for the Co-FER and Fe-FER models. The calculated barriers ΔE_{ACT1} of splitting dioxygen (Table 1 and Figures 1 and 3) are almost identical (24 and 25 kcal/mol, respectively) while the reaction energy of the reaction from **1** + O_2(g) to give **4** (Table 1 and Figures 1 and 3) significantly differs (−13 and −25 kcal/mol, respectively). Because of the very similar reaction barriers, splitting dioxygen over the distant binuclear Co(II) and Fe(II) centers should be similarly fast.

The cleavage of dioxygen for the Mn-FER model is more complicated since two spin changes occur during the course of the reaction. The spin state of **1** is $S = 10/2$ but upon adsorption of dioxygen the distant binuclear center undergoes a spin crossover to yield **2** or **3** with $S = 8/2$. **TS** ($S = 8/2$) also lies on one potential energy surface together with **2** and **3**. The calculated barrier of 37 kcal/mol (Table 1 and Figure 2) is
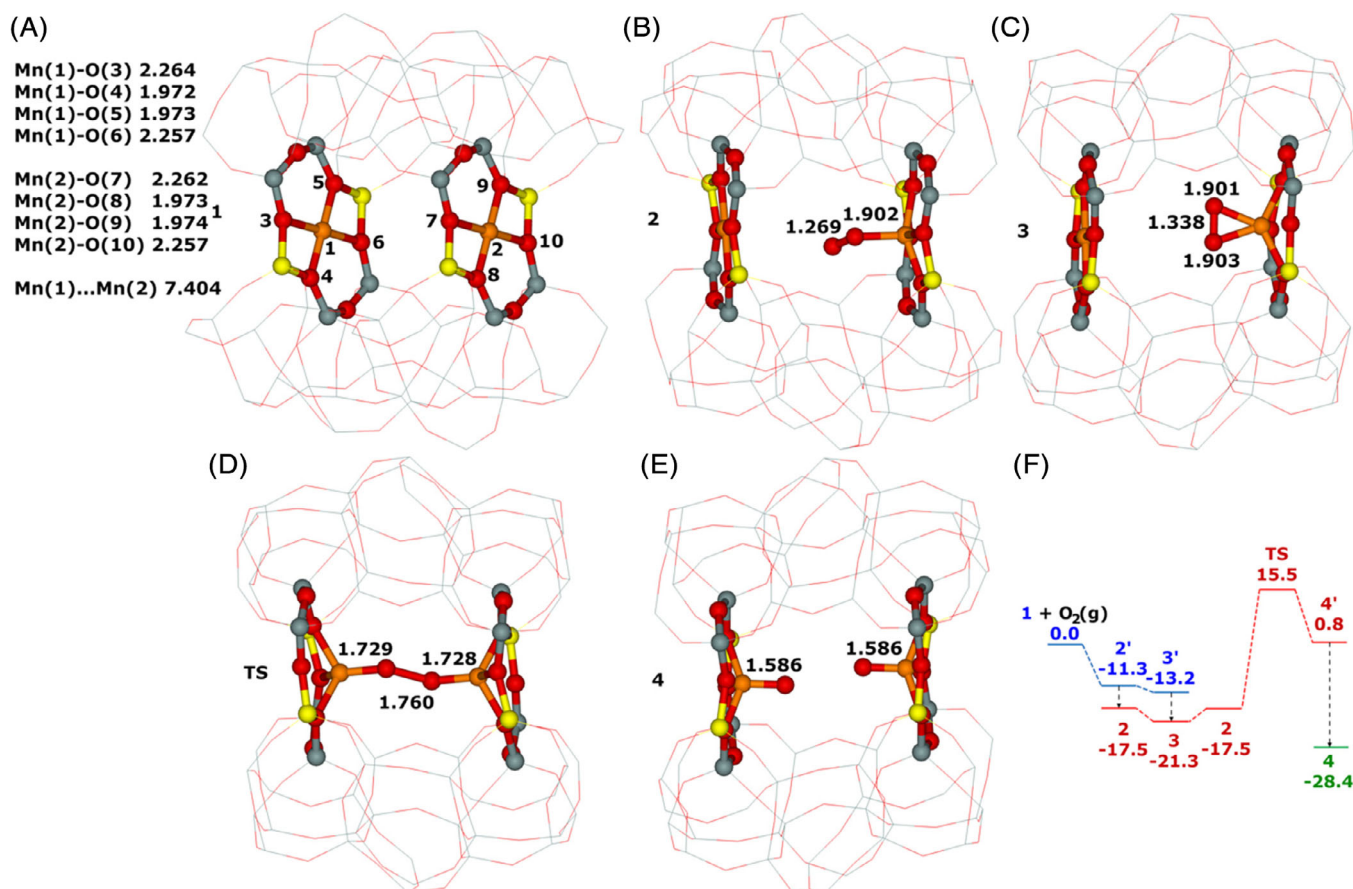
FIGURE 2 Mn-FER model. Optimized structures for (A) the two adjacent $\beta 2$ sites of Mn-ferrierite **1** ($S = 10/2$) after molecular dynamics (MD) simulations, (B) the monodentate [Mn OO$_{mono}$...Mn] complex **2** ($S = 8/2$), (C) the bidentate [Mn OO$_{bi}$...Mn] complex **3** ($S = 8/2$), (D) the [Mn—O—O—Mn] transition state **TS** ($S = 8/2$), and (E) the [Mn=O O=Mn] product **4** ($S = 6/2$). The distances are in Å. Silicon atoms are in gray, oxygen atoms in red, aluminum atoms in yellow, and manganese atoms in orange. Schematic energy profile (in kilocalorie per mol) for the spin states $S = 10/2$ blue profile, $S = 8/2$ red profile, and $S = 6/2$ green profile for (F) the formation of the Mn=O O=Mn product **4**

significantly higher by 12 kcal/mol that those calculated for the Co-FER and Fe-FER models indicating that the splitting dioxygen over the distant binuclear Mn(II) centers should be markedly slower relative to Co(II) and Fe(II). When a pair of the α-oxygen species is formed, the distant binuclear center undergoes another spin change since **4** has its ground state $S = 6/2$. We also localized the corresponding transition state with $S = 6/2$ but it is higher in energy that the TS with $S = 8/2$ by 10 kcal/mol. The cleavage of dioxygen over the distant binuclear Mn(II) center is the most exothermic among the three investigated cations.

The barrier of the cleavage of dioxygen predominantly determines the activity in splitting dioxygen which in turn is essential for tuning the zeolite systems with the distant binuclear M(II) centers as catalysts for the direct oxidation of methane. Nevertheless, the recombination of dioxygen has to be taken in the account as well. The corresponding energy barrier is included in Table 1. The reverse barrier ΔE_{ACT2} correlates well with the barrier ΔE_{ACT1} of splitting dioxygen (Table 1). The ΔE_{ACT2} values are larger than the ΔE_{ACT1} ones by 3 (Co-FER and Fe-FER) – 7 (Mn-FER) kcal/mol (i.e., the $\Delta\Delta E_{ACT}$ values in Table 1). The $\Delta\Delta E_{ACT}$ values also correspond to the difference in stability of the product **4** and the bidentate complex **3**. Since **4** is more stable than the bidentate complex **3** by 3 kcal/mol or more for all the three cations (Table 1), the equilibrium is strongly shifted toward the product **4** establishing essentially the exclusive presence of **4** in the zeolite after the oxidation of the Fe(II) cations by dioxygen.

The results discussed above show that the capability of splitting dioxygen is most likely general for the distant binuclear M(II) sites capable of the M(II) → M(IV) redox cycle proposing the possibility of developing M-zeolite based systems for the activation of dioxygen employed for direct oxidations using other transition metal cations than Fe.

The tendency of Fe(II) cations in zeolite matrices to form Fe oxides is well known and can represent a limitation on the preparation of highly active (i.e., with high Fe loadings) and stable systems for the activation of dioxygen, and subsequently, the oxidation of methane. The possibility of replacing Fe(II) by other more stable cations (e.g., Co(II) ones) represents a good starting point for the development of technologically applicable systems. Moreover, employing various M(II) cations able to perform the M(II) → M(IV) redox cycle may allow the optimization of the properties of the catalytic system toward the direct oxidation of methane and other molecules of interest using dioxygen.
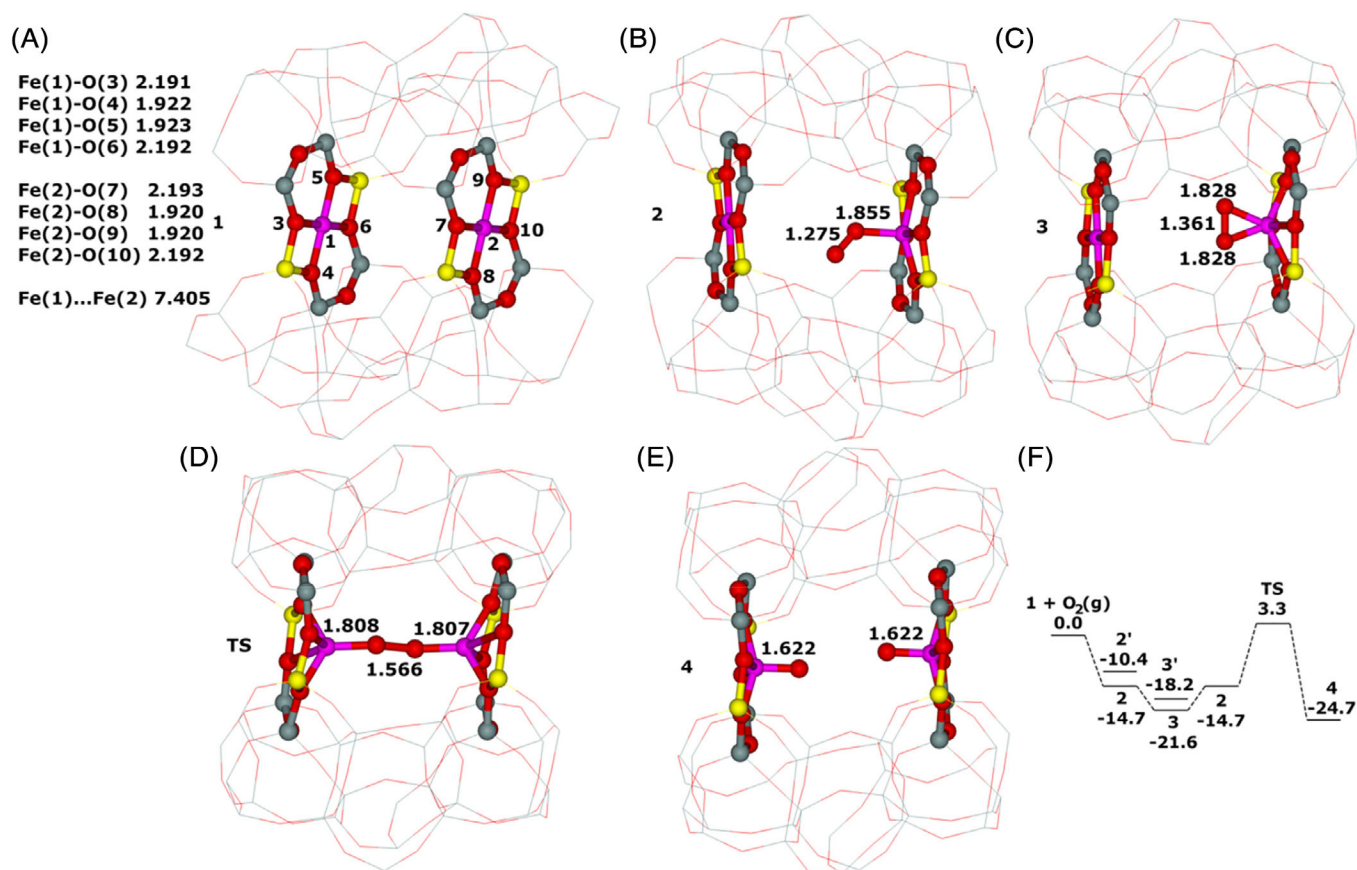
FIGURE 3 Fe-FER model. Optimized structures for (A) the two adjacent $\beta2$ sites of Fe-ferrierite **1** after molecular dynamics (MD) simulations, (B) the monodentate [Fe OO_{mono}...Fe] complex **2**, (C) the bidentate [Fe OO_{bi}...Fe] complex **3**, (D) the [Fe—O—O—Fe] transition state **TS**, and (E) the [Fe=O O=Fe] product **4**. The distances are in Å. Silicon atoms are in gray, oxygen atoms in red, aluminum atoms in yellow, and iron atoms in violet. Schematic energy (in kilocalorie per mol) profile for the spin state $S = 8/2$ (2′ and 3′ are $S = 10/2$) for (F) the formation of the Fe=O O=Fe product **4**

5 | CONCLUSIONS

The distant binuclear cationic Fe(II) centers in Fe-ferrierite were shown to split dioxygen at room temperature and directly oxidize methane to methanol at room temperature as well. Theoretical modeling clearly shows that this breakthrough in the activation of dioxygen is not limited exclusively to Fe(II) cations but the ability of dioxygen splitting represents a general property of the distant binuclear M(II) centers capable of the M(II) → M(IV) redox cycle with the M...M distance of ca 7.4 Å stabilized in M-ferrierite. Our results reveal that the distant binuclear M(II) (M(II) = Co(II), Mn(II), and Fe(II)) sites located in two adjacent β sites of ferrierite can split dioxygen and form a pair of the α-oxygen species which were reported to be very active in the oxidation of methane to methanol. This suggests the possibility of developing M-zeolite based tunable systems for the activation of dioxygen for direct oxidations using various transition metal cations in various zeolite matrices.

AUTHOR CONTRIBUTIONS
Jiri Dedecek: Conceptualization; formal analysis; funding acquisition; investigation; methodology; writing-original draft. **Edyta Tabor:** Conceptualization; formal analysis; validation; writing-original draft. **Prokopis C. Andrikopoulos:** Conceptualization; investigation; methodology; writing-original draft. **Stepan Sklenak:** Conceptualization; data curation; formal analysis; investigation; methodology; project administration; software; supervision; validation; writing-original draft; writing-review and editing.

DATA AVAILABILITY STATEMENT

The data that support the findings of this study are available from the corresponding author upon reasonable request.

ORCID

Stepan Sklenak https://orcid.org/0000-0003-4862-857X

REFERENCES

[1] B. E. R. Snyder, P. Vanelderen, M. L. Bols, S. D. Hallaert, L. H. Bottger, L. Ungur, K. Pierloot, R. A. Schoonheydt, B. F. Sels, E. I. Solomon, *Nature* **2016**, *536*, 317.

[2] K. Narsimhan, K. Iyoki, K. Dinh, Y. Roman-Leshkov, *ACS Cent. Sci.* **2016**, *2*, 424.

[3] K. T. Dinh, M. M. Sullivan, P. Serna, R. J. Meyer, M. Dinca, Y. Roman-Leshkov, *ACS Catal.* **2018**, *8*, 8306.

[4] E. Tabor, J. Dedecek, K. Mlekodaj, Z. Sobalik, P. C. Andrikopoulos, S. Sklenak, *Sci. Adv.* **2020**, *6*, eaaz9776.

[5] B. E. R. Snyder, M. L. Bols, R. A. Schoonheydt, B. F. Sels, E. I. Solomon, *Chem. Rev.* **2018**, *118*, 2718.

[6] J. H. Lee, W. Bonte, S. Corthals, F. Krumeich, M. Ruitenbeek, J. A. van Bokhoven, *Ind. Eng. Chem. Res.* **2019**, *58*, 5140.

[7] A. J. Knorpp, M. A. Newton, S. C. M. Mizuno, J. Zhu, H. Mebrate, A. B. Pinar, J. A. van Bokhoven, *Chem. Commun.* **2019**, *55*, 11794.

[8] V. L. Sushkevich, R. Verel, J. A. van Bokhoven, *Angew. Chem., Int. Ed* **2020**, *59*, 910.

[9] V. L. Sushkevich, J. A. van Bokhoven, *Catal. Sci. Technol.* **2020**, *10*, 382.

[10] M. A. Newton, A. J. Knorpp, V. L. Sushkevich, D. Palagin, J. A. van Bokhoven, *Chem. Soc. Rev.* **2020**, *49*, 1449.

[11] G. I. Panov, I. Sobolev, A. S. Kharitonov, *J. Mol. Catal.* **1990**, *61*, 85.

[12] S. Yuan, Y. Li, J. Peng, Y. M. Questell-Santiago, K. Akkiraju, L. Giordano, D. J. Zheng, S. Bagi, Y. Roman-Leshkov, Y. Shao-Horn, *Adv. Energy Mater.* **2020**, *10*, 2002154.

[13] K. Jisa, J. Novakova, M. Schwarze, A. Vondrova, S. Sklenak, Z. Sobalik, *J. Catal.* **2009**, *262*, 27.

[14] S. Sklenak, P. C. Andrikopoulos, B. Boekfa, B. Jansang, J. Novakova, L. Benco, T. Bucko, J. Hafner, J. Dedecek, Z. Sobalik, *J. Catal.* **2010**, *272*, 262.

[15] E. Tabor, M. Lemishka, Z. Sobalik, K. Mlekodaj, P. C. Andrikopoulos, J. Dedecek, S. Sklenak, *Commun. Chem.* **2019**, *2*, 71.

[16] K. A. Dubkov, V. I. Sobolev, G. I. Panov, *Kinet. Catal.* **1998**, *39*, 72.

[17] K. A. Dubkov, E. A. Paukshtis, G. I. Panov, *Kinet. Catal.* **2001**, *42*, 205.

[18] D. P. Ivanov, V. I. Sobolev, G. I. Panov, *Appl. Catal., A* **2003**, *241*, 113.

[19] I. Yuranov, D. A. Bulushev, A. Renken, L. Kiwi-Minsker, *Appl. Catal., A* **2007**, *319*, 128.

[20] M. L. Bols, S. D. Hallaert, B. E. R. Snyder, J. Devos, D. Plessers, H. M. Rhoda, M. Dusselier, R. A. Schoonheydt, K. Pierloot, E. I. Solomon, B. F. Sels, *J. Am. Chem. Soc.* **2018**, *140*, 12021.

[21] J. Dedecek, M. J. Lucero, C. Li, F. Gao, P. Klein, M. Urbanova, Z. Tvaruzkova, P. Sazama, S. Sklenak, *J. Phys. Chem. C* **2011**, *115*, 11056.

[22] J. Dedecek, Z. Sobalik, B. Wichterlova, *Catal. Rev. Sci. Eng.* **2012**, *54*, 135.

[23] J. Dedecek, E. Tabor, S. Sklenak, *ChemSusChem* **2019**, *12*, 556.

[24] S. Sklenak, P. C. Andrikopoulos, S. R. Whittleton, H. Jirglova, P. Sazama, L. Benco, T. Bucko, J. Hafner, Z. Sobalik, *J. Phys. Chem. C* **2013**, *117*, 3958.

[25] http://www.iza-structure.org/databases (accessed: February 25, 2020).

[26] I. J. Pickering, P. J. Maddox, J. M. Thomas, A. K. Cheetham, *J. Catal.* **1989**, *119*, 261.

[27] G. Kresse, J. Hafner, *Phys. Rev. B* **1993**, *48*, 13115.

[28] G. Kresse, J. Hafner, *Phys. Rev. B* **1994**, *49*, 14251.

[29] G. Kresse, J. Furthmuller, *Phys. Rev. B* **1996**, *54*, 11169.

[30] G. Kresse, J. Furthmuller, *Comput. Mater. Sci.* **1996**, *6*, 15.

[31] P. E. Blochl, *Phys. Rev. B* **1994**, *50*, 17953.

[32] G. Kresse, D. Joubert, *Phys. Rev. B* **1999**, *59*, 1758.

[33] J. P. Perdew, K. Burke, M. Ernzerhof, *Phys. Rev. Lett.* **1996**, *77*, 3865.

[34] S. N. Steinmann, C. Corminboeuf, *J. Chem. Theory Comput.* **2011**, *7*, 3567.

[35] S. N. Steinmann, C. Corminboeuf, *J. Chem. Phys.* **2011**, *134*, 044117.

[36] S. Grimme, *J. Comput. Chem.* **2004**, *25*, 1463.

[37] S. Nose, *J. Chem. Phys.* **1984**, *81*, 511.

[38] L. Verlet, *Phys. Rev.* **1967**, *159*, 98.

[39] L. Verlet, *Phys. Rev.* **1968**, *165*, 201.

[40] P. Klein, J. Dedecek, H. M. Thomas, S. R. Whittleton, V. Pashkova, J. Brus, L. Kobera, S. Sklenak, *Chem. Commun.* **2015**, *51*, 8962.

[41] R. Karcz, J. Dedecek, B. Supronowicz, H. M. Thomas, P. Klein, E. Tabor, P. Sazama, V. Pashkova, S. Sklenak, *Chem. – Eur. J.* **2017**, *23*, 8857.

[42] P. Sazama, J. Moravkova, S. Sklenak, A. Vondrov, E. Tabor, G. Sadovska, R. Pilar, *ACS Catal.* **2020**, *10*, 3984.